Proceedings of the Canadian Society for Mechanical Engineering International Congress
32nd Annual Conference of the Computational Fluid Dynamics Society of Canada
Canadian Society of Rheology Symposium
CSME-CFDSC-CSR 2025
May 25–28, 2025, Montréal, Québec, Canada

Unsteady wake characteristics of a plunging airfoil at post-stall conditions

Fahimeh Goodarzi[1*], Giuseppe Di Labbio[1], Mahmoud Mani[2]
[1]Department of Mechanical Engineering, École de technologie supérieure (ÉTS), Montréal, QC, Canada
[2]Department of Aerospace Engineering, Amirkabir University of Technology, Tehran, Iran
*fahimeh.goodarzi.1@ens.etsmtl.ca

Abstract — The unsteady wake characteristics of a plunging airfoil were investigated experimentally during near-stall and post-stall conditions for an Eppler 361 airfoil at Reynolds number Re = 2.5×10^4. Oscillation frequencies of 1.0 Hz and 3.0 Hz (reduced frequencies k = 0.19 and 0.57, respectively) are considered for a total plunging depth of 16 cm ($1.07c$) and three different initial angles of attack (α_0 = 0°, 10°, 15°). The results show that the leading- and trailing-edge vortices have a more dominant effect on the wake velocity for initial angles of attack both near (α_0 = 10°) and post (α_0 = 15°) stall of the airfoil. The results show periodic variations in wake velocity with notably different behaviour in the lower portion of the wake between near and post stall cases. For the post-stall condition, the wake velocity experiences clearly periodic larger fluctuations in the center of wake, indicative of periodic vortex shedding. The unsteady flow field of a plunging airfoil exhibits hysteresis effects, forming a closed loop in the velocity-position diagram with differing velocity magnitudes between the upstroke and downstroke motions. The reduced frequency has a significant influence on wake velocity and therefore on aerodynamic loads.

Keywords: unsteady wake; reduced frequency; post-stall; plunging airfoil; leading-edge vortices; trailing-edge vortices

I. INTRODUCTION

Unsteady aerodynamics, such as transient gust loads on aircraft or the wake characteristics of an oscillating airfoil, can enhance our understanding of several complex flow phenomena (e.g., separation, reattachment, vortex shedding) observed in nature (e.g., aquatic and avian animal locomotion) [1], energy production (e.g., hydraulic and wind turbines) and transportation (e.g., micro air vehicles, helicopter blades) [2,3].

Several studies have investigated the unsteady aerodynamics of oscillating airfoils and flapping wings [4], with von Kármán and Burgers [5] presenting an early theory on the effects of wake vortices behind airfoils on drag and thrust. Subsequent studies have demonstrated that pitching and plunging airfoils generate a von Kármán vortex street at low airfoil oscillation frequencies. The vortices shed from the upper airfoil surface rotate clockwise, while those shed from the lower surface rotate counterclockwise. Under these conditions, the velocity profile in the wake exhibits a velocity deficit or drag. At higher airfoil oscillation frequencies, the oscillating airfoil generates a reverse von Kármán vortex street, where the vortices shed from the upper surface rotate counterclockwise and those shed from the lower surface clockwise. The velocity profiles in this case instead indicate thrust production in the wake [6-10].

Although numerical and experimental studies of oscillating airfoil motions combining pitching and plunging have revealed additional key parameters as well as more complex vortex interactions and lift/drag production [11], it is interesting that a plunging airfoil alone demonstrates all the essential fluid dynamics of oscillating airfoils. These include vortex shedding, trailing- and leading-edge vortices [12], leading-edge separation at high oscillation frequencies and plunging amplitudes, as well as drag or thrust generation under specific conditions [13].

When the angle of attack of an oscillating airfoil exceeds the static stall angle, flow separation or stall begins later compared to a static airfoil. This delay is accompanied by the formation of a leading-edge vortex on the airfoil surface, which moves downstream [14,15]. At a high angle of attack, a plunging airfoil produces strong leading-edge vortices accompanied by complex vortex interactions in the wake. While the leading-edge vortex temporarily enhances lift by remaining attached to the surface, its eventual movement past the trailing-edge generates a significant negative, or nose-down, pitching moment and induces flow separation across the entire airfoil. This unsteady phenomenon is referred to as dynamic stall and can result in structural fatigue and potential failure due to intense vibrations and excessively high aerodynamic loads [15]. Nonetheless, the increase in lift of the airfoil in the post-stall and dynamic stall regimes can be used for flow control strategies [16]. Flow visualization studies of an oscillating airfoil in the dynamic stall regime at high angles of attack also show the formation of leading- and trailing-edge vortices [17]. Gao et al. [18] identified that the interaction patterns among consecutive leading-edge vortices and the trailing-edge vortices constitute the main mechanisms influencing the three-dimensional transition and the related force characteristics of an oscillating airfoil. Bull et al.

[3] also observed significant load fluctuations at post-stall angles of attack during plunging motions (with increasing and decreasing equivalent angle of attack) attributed to large-scale vortex shedding alternating from the leading and trailing edges.

For flights at low Reynolds numbers (Re < 10^6), designers face challenges in overcoming poor performance caused by flow separation. One possible solution is to operate at high angles of attack to generate more lift. However, this can lead to post-stall conditions during maneuvers and when encountering gusts [19]. Certain unsteady parameters, such as oscillation frequency and amplitude, can have a positive effect on lift during post-stall and influence the behaviour of the leading- and trailing-edge vortices [20]. Despite the important role of leading-edge vortices on aerodynamic loads and in the wake, the behaviour of leading- and trailing-edge vortices under various unsteady conditions at high angles of attack, as well as their effects on the unsteady wake of oscillating airfoils, are still not completely understood.

In this study, we measure the unsteady wake characteristics of an Eppler 361 airfoil performing pure plunging motions at various angles of attack, including both pre-stall and post-stall conditions, at a low Reynolds number (Re = 2.5×10^4). Of particular interest are the effects of leading-edge vortices and oscillation frequency on the unsteady wake, including velocity hysteresis. The experimental conditions are selected to closely replicate those experienced during civil aircraft maneuvers and gust encounters. Hot-wire anemometry is used to measure the velocity in the wake.

II. Methodology

The experiments were conducted in a closed circuit low-speed wind tunnel at the Amirkabir University of Technology, having a rectangular test section of 0.45 m × 0.45 m and a length of 1.2 m. The turbulence intensity in the test section is 0.1%, and the maximum wind tunnel speed in the test section is 45 m/s. An Eppler 361 airfoil, made of solid aluminum, with a chord length (c) of 15 cm and a span of 45 cm, was placed horizontally in the test section. The gap between the airfoil and the side walls was less than 0.1 cm.

The scotch-yoke mechanism was used to create the plunging motion. Figure 1 shows a schematic of the mechanism which includes a variable speed motor that can provide oscillating

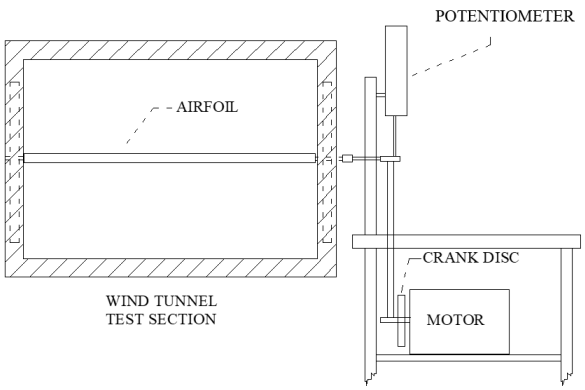

Figure 1: Schematic of the mechanical system used to create the plunging motion of the airfoil.

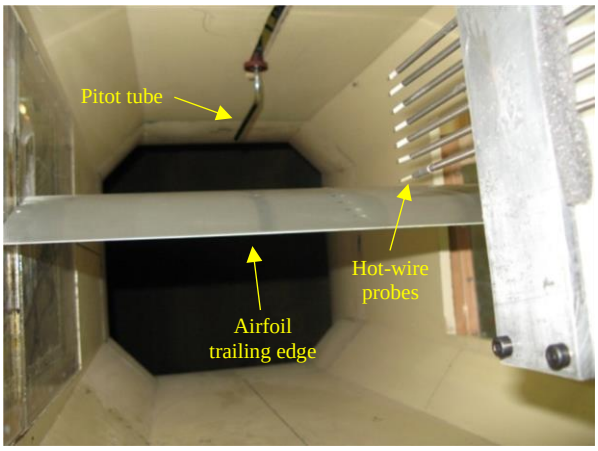

Figure 2: Hot-wire array behind the Eppler 361 airfoil.

motions with frequencies (f) ranging from 1.0 Hz to 3.0 Hz and plunging amplitudes (h_0) ranging from 4 cm to 8 cm. In this work, we only discuss the largest plunging motion (total plunging depth, normalized by the chord, $\bar{h} = 2h_0/c = 1.07$). The corresponding Reynolds number, based on the freestream velocity of U = 2.5 m/s, was Re = 2.5×10^4. Three initial angles of attack (α_0) were investigated, namely, 0°, 10° and 15° at reduced frequencies ($k = \pi fc/U$) of 0.19 (1.0 Hz) and 0.57 (3.0 Hz). Velocity measurements were acquired using constant temperature anemometry (CTA) and seven 5-µm hot-wire probes.

A traverse mechanism was used to move the series of hot-wires through the near wake both vertically ($y/c = \pm1$) and downstream. The velocity was measured up to one chord length downstream of the trailing edge of the airfoil ($x/c \leq 1$). Figure 2 shows the series of hot-wire probes and the airfoil within the wind tunnel test section. The hot-wire measurements were calibrated in the wind tunnel before each experiment to minimize errors caused by changes in sensor temperature. A Pitot tube measures the freestream velocity.

The instantaneous angle of attack (α) is the sum of the initial angle of attack α_0 and the equivalent angle of attack α_{eq} =

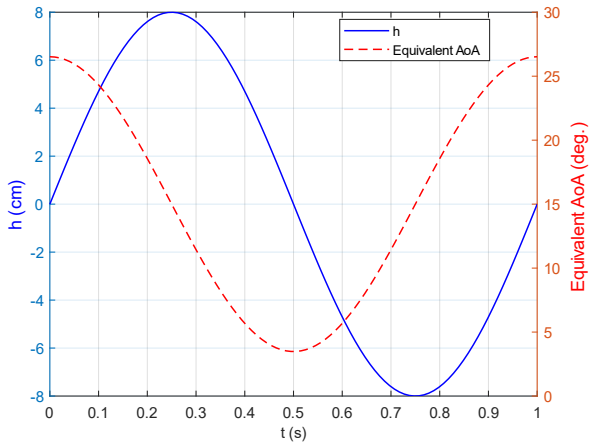

Figure 3: Variation of airfoil height in cm (blue, solid) and equivalent angle of attack (red, dashed) during one plunging cycle for α_0 = 0° and k = 0.19.

$k\bar{h}\cos(2\pi ft)$, namely, $\alpha = \alpha_0 + \alpha_{eq}$ where the parameters k and $\bar{h}$ ultimately transmit the effects of the plunging motion on the instantaneous angle of attack and t is in seconds. Likewise, the dimensional airfoil height is given by $h = h_0 \sin(2\pi ft)$, as measured from the point at which the oscillation mechanism is attached ($0.25c$ from the leading edge).

The phase lag between the plunging motion and the equivalent angle of attack is $\pi/2$ radians. Figure 3 shows a schematic of the plunging airfoil motion for $\bar{h}$ = 1.07, α_0 = 0° and k = 0.19, as well as the corresponding variation of the equivalent angle of attack over one cycle. The equivalent angle of attack reaches its maximum or minimum value when the airfoil height h = 0 cm, namely, when the airfoil is in its neutral position during the upstroke or downstroke phase respectively. The plunging motion of an airfoil affects the equivalent angle of attack by decreasing it above the neutral position and increasing it below the neutral position. These variations become especially significant near the static stall angle of attack and post-stall.

III. Results & Discussion

To explore the effects of the leading- and trailing-edge vortices on velocity in the unsteady wake, we present the velocity measurements in three separate regimes, namely, before the static stall angle of attack (α_0 = 0°) in section III.A, near the static stall angle of attack (α_0 = 10°) in section III.B, and after the static stall angle of attack (α_0 = 15°) in section III.C. In section III.D, we examine the ensemble-averaged velocity hysteresis in the wake. To illustrate the wake behaviour, the wake velocity is measured at several positions, though we restrict our discussion here to those taken one chord length downstream of the trailing edge (x/c = 1) at three vertical positions as shown in Fig. 4, representing the upper wake (point a, y/c = 0.5), the middle wake (point b, y/c = 0) and the lower wake (point c, y/c = -0.5) with reference to the neutral airfoil position (h = 0 cm).

A. *Before the static stall angle of attack*

In this section, we consider an initial angle of attack α_0 = 0°. Figure 5 shows the velocity in the middle portion of the wake (Fig. 4, point b) for reduced frequencies of k = 0.19 (left) and k = 0.57 (right) over one cycle. The airfoil position is shown for reference as a red dashed line. Leading-edge vortices are known to develop, detach and shed in the wake even at low angles of attack when the reduced frequencies are sufficiently high [20]. At the low reduced frequency (k = 0.19), the flow remains largely laminar though we already observe velocity fluctuations as the airfoil passes through its neutral position, both during its upstroke and downstroke. Such velocity fluctuations can generally result from flow perturbations induced by the motion of the airfoil itself, from the shedding of a small leading-edge vortex in the wake during the downstroke, or from the influence of trailing-edge vortices shed as the airfoil passes through its neutral position. At the higher reduced frequency (k = 0.57), the velocity fluctuations are more apparent and peak during the downstroke motion as the airfoil passes through the neutral position (h = 0 cm) and the equivalent angle of attack begins to increase. An overall increase in peak velocity magnitude is also observed.

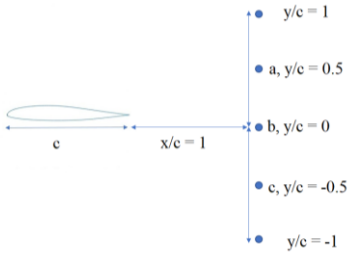

Figure 4: Schematic of the velocity measurement points, relative to the neutral position, at one chord length downstream (x/c = 1) including point a in the upper wake (y/c = 0.5), point b in the middle wake (y/c = 0), and point c in the lower wake (y/c = -0.5).

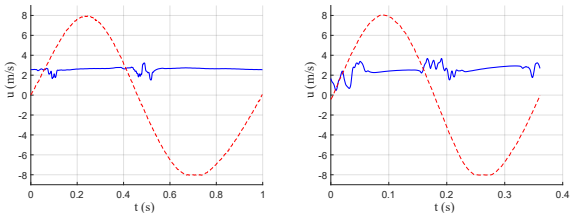

Figure 5: Velocity variations over one cycle at the middle portion of the wake (Fig. 4, point b) where x/c = 1 and y/c = 0 as measured from the trailing edge and with reference to the neutral position. The initial angle of attack is α_0 = 0°. The reduced frequency (k) is 0.19 on the left and 0.57 on the right. The dashed red line shows the airfoil position as a reference.

Figure 6 shows the velocity measurements in the upper wake (Fig. 4, point a) at the same reduced frequencies. At the lower reduced frequency (k = 0.19), the velocity is observed to exhibit a low amplitude variation following the airfoil's displacement in time. This is consistent with the shedding of a small leading-edge vortex. An increase in velocity is first observed in the upper wake (just prior to t = 0.4 s) after which we observe its effects in the middle wake (Fig. 5, left). At k = 0.19, the wake only extends as far as $|y/c|$ = 0.5. At the higher reduced frequency (k = 0.57), the velocity exhibits considerable excursions throughout the entire cycle, which is consistent with the shedding of a leading-edge vortex as the airfoil descends from its uppermost position, which is felt one chord downstream only as the airfoil ascends to its neutral position [22-24]. The wake also widens considerably, extending beyond the measurement points (i.e., $|y/c| \gg 1$).

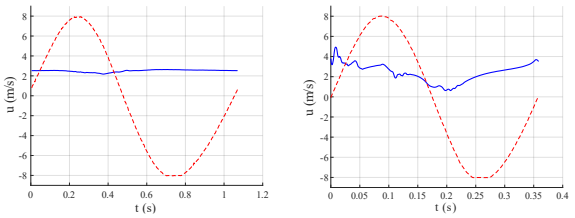

Figure 6: Velocity variations over one cycle at the upper portion of the wake (Fig. 4, point a) where x/c = 1 and y/c = 0.5 as measured from the trailing edge and with reference to the neutral position. The initial angle of attack is α_0 = 0°. The reduced frequency (k) is 0.19 on the left and 0.57 on the right. The dashed red line shows the airfoil position as a reference.

B. *Near the static stall angle of attack*

In this section, we consider an initial angle of attack of α_0 = 10°, which is close to the static stall angle of attack of the airfoil (α_{stall} = 12.5°). Figure 7 shows the velocity variations over two cycles for a reduced frequency of k = 0.57 at the upper (top), middle (center) and lower (bottom) portions of the wake, corresponding to y/c = 0.5, 0 and -0.5 respectively (as in Fig. 4). In comparison to the higher reduced frequency (k = 0.57) results with a low initial angle of attack (α_0 = 0°) presented in Figs. 5 and 6, the velocity fluctuations are more significant and exhibit clear periodicity at all measured portions of the wake. Gao et al. [18] observed that at high initial angle of attack (α_0) and reduced frequency (k), which causes the instantaneous angle of attack (α) during upward motion to be significantly higher than that during downward motion, there is considerably weaker vortex shedding from the lower surface of the airfoil and the wake is primarily influenced by the leading-edge vortex from the upper surface. The behaviour of the velocity fluctuations is therefore indicative of the shedding of leading-edge vortices in the wake, namely, as the airfoil descends from its uppermost position (h = 8 cm) down to its neutral position (h = 0 cm), a large vortex is shed and its effects are felt at roughly the same time at the three measurement points as the airfoil begins its ascent. The passage of the leading-edge vortex is however more clearly observed in the upper portion of the wake where it is shed.

C. *After static stall angle of attack*

In this section, we consider an initial angle of attack of α_0 = 15°, which is close to and exceeds the static stall angle of attack of the airfoil (α_{stall} = 12.5°). At the plunging amplitude of study ($\bar{h}$ = 1.07) and the lowest initial angle of attack (α_0 = 0°), the maximum instantaneous angle of attack varies from 11.5° to 34.6° when k = 0.19 and 0.57 respectively. At an initial angle of

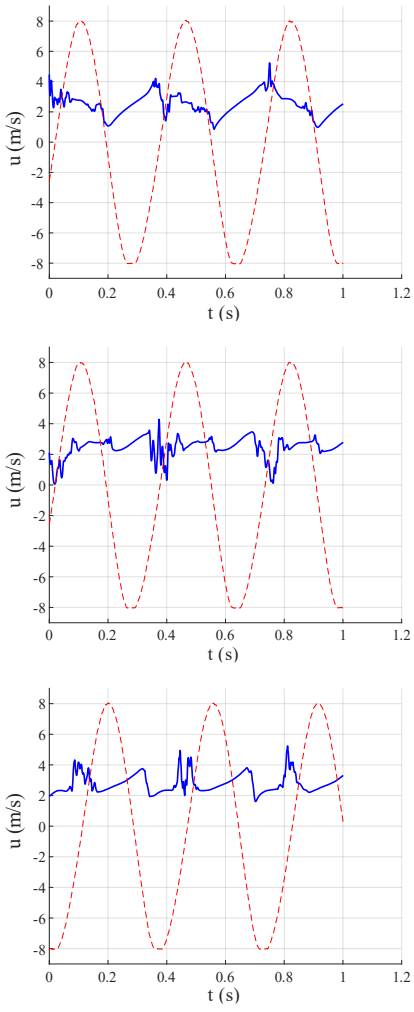

Figure 7: Velocity variations over two cycles at the upper portion of the wake (Fig. 4, point a) where x/c = 1 and y/c = 0.5 as measured from the trailing edge and with reference to the neutral position, the middle portion (Fig. 4, point b) where y/c = 0, and the lower portion (Fig. 4, point c) where y/c = -0.5. The initial angle of attack is α_0 = 10° and the reduced frequency (k) is 0.57. The dashed red line shows the airfoil position as a reference.

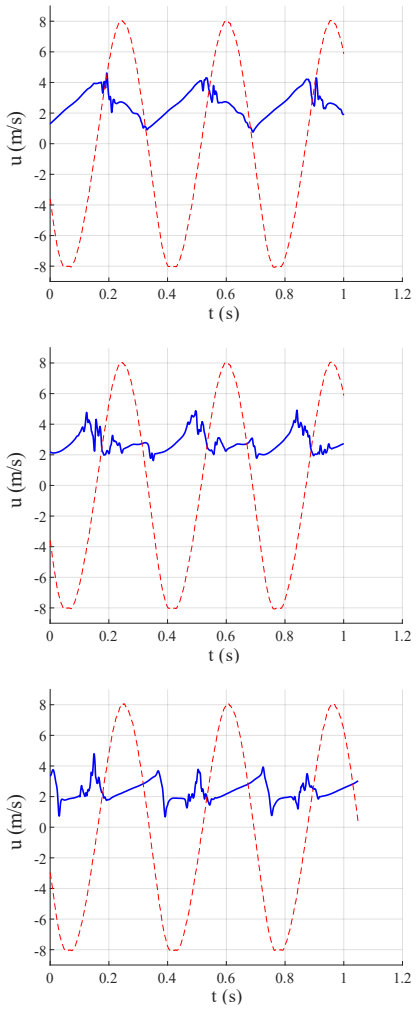

Figure 8: Velocity variations over two cycles at the upper portion of the wake (Fig. 4, point a) where x/c = 1 and y/c = 0.5 as measured from the trailing edge and with reference to the neutral position, the middle portion (Fig. 4, point b) where y/c = 0, and the lower portion (Fig. 4, point c) where y/c = -0.5. The initial angle of attack is α_0 = 15° and the reduced frequency (k) is 0.57. The dashed red line shows the airfoil position as a reference.

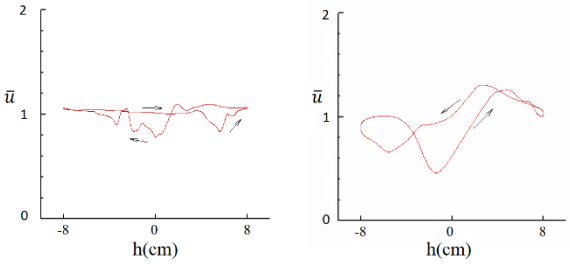

Figure 9: Ensemble-averaged velocity hysteresis over one cycle at the middle portion of the wake (Fig. 4, point b) where x/c = 1 and y/c = 0 as measured from the trailing edge and with reference to the neutral position. The initial angle of attack is α_0 = 0°. The reduced frequency (k) is 0.19 on the left and 0.57 on the right.

attack of α_0 = 15°, the maximum instantaneous angle of attack attains 49.6° at k = 0.57, which far surpasses the static stall angle. We therefore expect to have a deep dynamic stall. The dynamic stall process is commonly divided into four stages: attached flow over the airfoil surface at low angles of attack, the formation of a strong leading-edge vortex, the detachment of this vortex from the airfoil's suction surface, and subsequent reattachment of the flow [1-3].

Figure 8 shows the velocity variation over two cycles at the higher reduced frequency of k = 0.57 at the upper (top), middle (center) and lower (bottom) portions of the wake, corresponding again to y/c = 0.5, 0 and -0.5 respectively (as in Fig. 4). In the upper wake (Fig. 4, point a), the velocity decreases during the airfoil's upstroke from the neutral position (i.e., while the equivalent angle of attack decreases) and begins to recover as the airfoil descends past the neutral position. In the lower wake (Fig. 4, point c), the velocity increase is somewhat less significant compared to the other locations. The largest velocity variation occurs during the second half of the plunging motion (i.e., while the equivalent angle of attack increases). The greatest time-averaged forces and moments have been shown to occur when the unsteady motion is within or near the post-stall flow regime of the static airfoil [20].

In the middle portion of the wake (Fig. 4, point b), we observe a gap between consecutive shedding of the leading-edge vortices that can be interpreted as a delay in the formation and propagation of the leading-edge vortex due to the higher reduced frequency. At reduced frequencies below 0.15, the process of

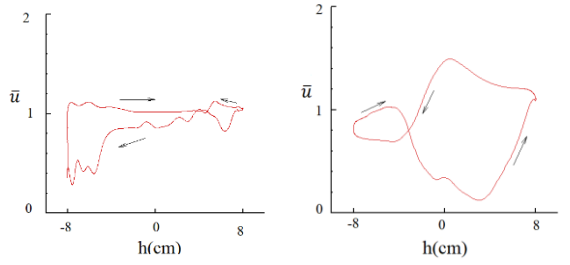

Figure 10: Ensemble-averaged velocity hysteresis over one cycle at the middle portion of the wake (Fig. 4, point b) where x/c = 1 and y/c = 0 as measured from the trailing edge and with reference to the neutral position. The initial angle of attack is α_0 = 10°. The reduced frequency (k) is 0.19 on the left and 0.57 on the right.

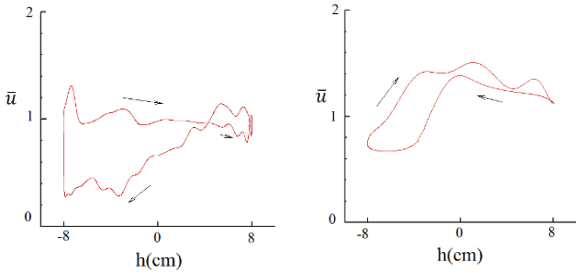

Figure 11: Ensemble-averaged velocity hysteresis over one cycle at the middle portion of the wake (Fig. 4, point b) where x/c = 1 and y/c = 0 as measured from the trailing edge and with reference to the neutral position. The initial angle of attack is α_0 = 15°. The reduced frequency (k) is 0.19 on the left and 0.57 on the right.

dynamic stall and subsequent shedding are similar to a typical bluff-body von Kármán vortex street, where multiple alternating vortices are released from the leading and trailing edges [23]. The velocity fluctuations at the lower reduced frequency of k = 0.19 (not shown) similarly shows the effect of multiple vortices in the wake.

D. Velocity hysteresis

At reduced frequencies k < 0.2, the dynamic stall vortex is shed before the maximum instantaneous angle of attack is reached, resulting in a small counterclockwise loop at the lower right-hand side of the larger clockwise loop in lift hysteresis [22]. In this study, we observe the same behaviour in velocity hysteresis. Figures 9-11 show the ensemble-averaged velocity hysteresis over one cycle at the middle portion of the wake (Fig. 4, point b) for each initial angle of attack (α_0 = 0°, 10° and 15° respectively). The velocity hysteresis profile shows a small counterclockwise loop at k = 0.19 at all angles of attack. When the initial angle of attack is zero (α_0 = 0°), the variations of velocity over one cycle show the combination of clockwise and counterclockwise variations, indicating the presence of vortices shedding in the wake and corresponding increases and decreases in velocity with the passage of the vortex through the measurement points. Increasing the reduced frequency induces larger leading-edge vortices, increasing the velocity fluctuations in the wake, resulting in a more open (larger loop) hysteresis pattern. As α_0 increases from 0° to 15°, the hysteresis loops involve stronger and larger vortical structures [16]. In the case of α_0 = 15° and k = 0.57, only a clockwise loop remains along with an overall increase in velocity magnitude and larger aerodynamic forces over the airfoil. The velocity hysteresis suggests that lift increases progressively as the airfoil moves from stall onset to the light stall regime, and finally to the deep stall regime.

IV. Conclusion

In this study, the unsteady wake of a plunging Eppler 361 airfoil was investigated at a Reynolds number of Re = 2.5×10^4 for a total plunging depth of $\bar{h}$ = 1.07. We considered reduced frequencies of k = 0.19 and 0.57 for three initial angles of attack representing pre-stall (α_0 = 0°), near stall (α_0 = 10°) and post-stall (α_0 = 15°) conditions. The velocity was measured through constant temperature hot-wire anemometry at one chord

downstream of the trailing edge in the upper (a half-chord above), middle and lower (a half-chord below) portions of wake with reference to the neutral position. Our results show that the oscillation frequency strongly influences wake characteristics of a plunging airfoil, which is consistent with the literature [2, 3, 13, 20, 23]. Previous studies focus mainly on the aerodynamic characteristics (e.g., lift) at low oscillation amplitudes and low frequencies. In our work, we examined the effects of a broader range of oscillation conditions and angles of attack on velocity variations across different regions in the wake, providing new insights into the wake dynamics under extreme oscillatory conditions.

Before the static stall angle of attack ($\alpha_0 = 0°$), the velocity in the wake shows small variations and smaller peaks, indicating that the boundary layer over the airfoil remains laminar. As the reduced frequency increases, the start of transition from laminar to turbulent flow, as well as its reversion, are delayed or even prevented, causing a slight decrease in the degree of hysteresis variations.

When the initial angle of attack ($\alpha_0 = 10°$) is near the static angle of attack of the airfoil ($\alpha_{\text{stall}} = 12.5°$), stall occurs during the downstroke. As the equivalent angle of attack of the airfoil increases, the flow separates from the upper surface and reattaches, forming a separation bubble. With further increase, a leading-edge vortex forms. At the same time, a weaker trailing-edge vortex develops from the lower surface. During the downstroke, the leading-edge vortex is carried downstream and sheds in the wake. Velocity variations in the wake and velocity hysteresis clearly identify the leading-edge vortex. In the middle portion of the wake, the velocity variations are more unsteady.

When the equivalent angle of attack exceeds its static stall angle, the boundary layer becomes more unsteady and the stall phenomenon intensifies. The reversed flow moves upward, leading to the formation of a larger and stronger leading-edge vortex. Increasing the reduced frequency delays the formation of the leading-edge vortex and subsequent ones. Although the vortex shedding phenomenon does not fundamentally change, its strength and phase are highly dependent on the reduced frequency. However, as the leading-edge vortex enters the wake, it has a marked effect on the velocity fluctuations, velocity hysteresis and overall wake thickness.

REFERENCES

[1] A. J. Smits, "Undulatory and oscillatory swimming," J. Fluid Mech., vol. 874, p. P1, 2019.

[2] W. Shyy et al., An Introduction to Flapping Wing Aerodynamics, Cambridge, U.K.: Cambridge University Press, 2013.

[3] S. Bull et al., "Unsteady aerodynamics of a plunging airfoil in transient motion," J. Fluids Struct., vol. 103, p. 103288, 2021.

[4] J. A. Ekaterinaris and M. F. Platzer, "Computational prediction of airfoil dynamic stall," Prog. Aerosp. Sci., vol. 33, no. 11–12, pp. 759–846, 1998.

[5] T. von Kármán and J. M. Burgers, General Aerodynamic Theory: Perfect Fluids, vol. 2, Berlin, Germany: Springer, 1935.

[6] B. Satyanarayana, "Unsteady wake measurements of airfoils and cascades," AIAA J., vol. 15, no. 5, pp. 613–618, 1977.

[7] C.-M. Ho and S.-H. Chen, "Unsteady wake of a plunging airfoil," AIAA J., vol. 19, no. 11, pp. 1492–1494, 1981.

[8] K. Jones, C. Dohring, and M. Platzer, "Wake structures behind plunging airfoils: A comparison of numerical and experimental results," in Proc. 34th AIAA Aerosp. Sci. Meet. Exhib., 1996.

[9] J. C. S. Lai and M. F. Platzer, "Jet characteristics of a plunging airfoil," AIAA J., vol. 37, no. 12, pp. 1529–1537, 1999.

[10] C. Chabalko et al., "Study of deflected wake phenomena by 2D unsteady vortex lattice," in Proc. 50th AIAA/ASME/ASCE/AHS/ASC Struct., Struct. Dyn. Mater. Conf., 17th AIAA/ASME/AHS Adapt. Struct. Conf., 11th AIAA, 2009.

[11] W. Shyy, Y. Lian, J. Tang, D. Viieru, and H. Liu, Aerodynamics of Low Reynolds Number Flyers. Cambridge, U.K.: Cambridge University Press, 2008.

[12] M. M. Koochesfahani, "Vortical patterns in the wake of an oscillating airfoil," AIAA J., vol. 27, no. 9, pp. 1200–1205, 1989.

[13] B. Turhan, Z. Wang, and I. Gursul, "Coherence of unsteady wake of periodically plunging airfoil," J. Fluid Mech., vol. 938, p. A14, 2022.

[14] J. G. Leishman, Principles of Helicopter Aerodynamics. Cambridge, U.K.: Cambridge University Press, 2000.

[15] K. Ramesh et al., "Discrete-vortex method with novel shedding criterion for unsteady aerofoil flows with intermittent leading-edge vortex shedding," J. Fluid Mech., vol. 751, pp. 500–538, 2014.

[16] I. Gursul, D. J. Cleaver, and Z. Wang, "Control of low Reynolds number flows by means of fluid-structure interactions," Prog. Aerosp. Sci., vol. 64, pp. 17–55, 2014.

[17] J. Panda and K. B. M. Q. Zaman, "Experimental investigation of the flow field of an oscillating airfoil and estimation of lift from wake surveys," J. Fluid Mech., vol. 265, pp. 65–95, 1994.

[18] A.-K. Gao et al., "Three-dimensional transition and force characteristics of low-Reynolds-number flows past a plunging airfoil," J. Fluid Mech., vol. 973, p. A43, 2023.

[19] Z. Zhang, Z. Wang, and I. Gursul, "Post-stall flow control with upstream flags," Exp. Fluids, vol. 63, no. 11, p. 179, 2022.

[20] O. Son et al., "Leading-edge vortex dynamics on plunging airfoils and wings," J. Fluid Mech., vol. 940, p. A28, 2022.

[21] M. Carta, R. Putzu, and T. Ghisu, "A comparison of plunging- and pitching-induced deep dynamic stall on an SD7003 airfoil using URANS and LES simulations," Aerosp. Sci. Technol., vol. 121, p. 107307, 2022.

[22] J. Panda and K. B. M. Q. Zaman, "Experimental investigation of the flow field of an oscillating airfoil and estimation of lift from wake surveys," J. Fluid Mech., vol. 265, pp. 65–95, 1994.

[23] D. Rival and C. Tropea, "Characteristics of pitching and plunging airfoils under dynamic-stall conditions," J. Aircraft, vol. 47, no. 1, pp. 80–86, 2010.

[24] F. Ajalli, M. Mani, and M. Tadjfar, "Plunging wake analysis of an airfoil equipped with a Gurney flap," Exp. Tech., vol. 39, pp. 48–60, 2015.